ESTIMATION OF HAWAIIAN ISLANDS FIRE FUEL PARAMETERS FROM HYPERSPECTRAL IMAGERY

Matthew L. Clark,[1] Dar A. Roberts,[1] Margaret E. Gardner,[1] and David R. Weise[2]

1. Introduction

Wildland fire has played a role in the development of some of the flora and fauna of the Hawaiian Islands given the volcanic nature of the archipelago's origin. However, the current floral and faunal composition of the major islands (Kaua'i, O'ahu, Moloka'i, Maui, and Hawai'i) is quite different from the biota that were present when humans first settled the islands circa 600 A.D. Large percentages of the land area on the major islands have been transformed by human activity, drastically altering fire regimes. For example, invasive non-native grass species have increased the occurrence and extent of wildland fire (D'Antonio and Vitousek, 1992). Fire can be detrimental to some native plants in Hawaii thereby jeopardizing survival and leading to loss of biodiversity (Mehrhoff, 1998). However, some native species appear to respond well to low intensity fires.

Fire behavior computer models are useful tools to understand the function of vegetative fuel types in propagating fire and predicting the effectiveness of fire management techniques in protecting and restoring native vegetation. These models (e.g., FARSITE (Finney, 1998)) require maps of fuel models, which are the quantitative description of the vegetation fuel bed in two or three dimensions. There is little vegetative fuels information available for the Hawaiian Islands. A recent advancement was the completion of the U.S. Forest Service stereo-photograph series and vegetation plots which quantitatively describe fuel properties in a range of grassland, shrubland, woodland and forest vegetation types at 36 sites across five of the islands (Wright et al., 2002).

Remote sensing has immense potential for fire behavior modeling in that it can provide larger extents and more frequent measurements of fuel-load parameters than what is currently available. The objectives of this study were to: 1) assess the utility of AVIRIS spectral features for per-pixel estimation of fuel parameters, and 2) compare the relative benefits of narrowband (i.e., AVIRIS) and broadband (i.e., Landsat ETM+) formulations of vegetation indices in estimating fuel properties.

2. Data acquisition and processing

The study was focused on the islands of Hawai'i, Kaua'i, Moloka'i, O'ahu and Maui in the Hawaiian archipelago (Fig. 1). Field data from 24 vegetation sampling plots (Fig. 1) were collected in November 1999, July 2000 and February 2001 (Wright et al., 2002). There were 9 grassland, 3 shrubland, 7 woodland and 5 tree-plantation plots sampled from 47 to 2037-m elevation. Tree plantations were dominated by *Casuarina equisetifolia*, *Pinus radiata*, *Pinus pinaster*, or *Pinus elliottii*. Thirteen of the plots were on Hawai'i island, mainly on the drier side of the precipitation gradient that runs from east to west across the island. Fuel parameters measured included percent canopy cover and the biomass of dead and live materials. Dead-wood biomass was classified into diameter classes: <0.64 cm, 0.65-2.5 cm, 2.6-7.6 cm and > 7.6 cm.

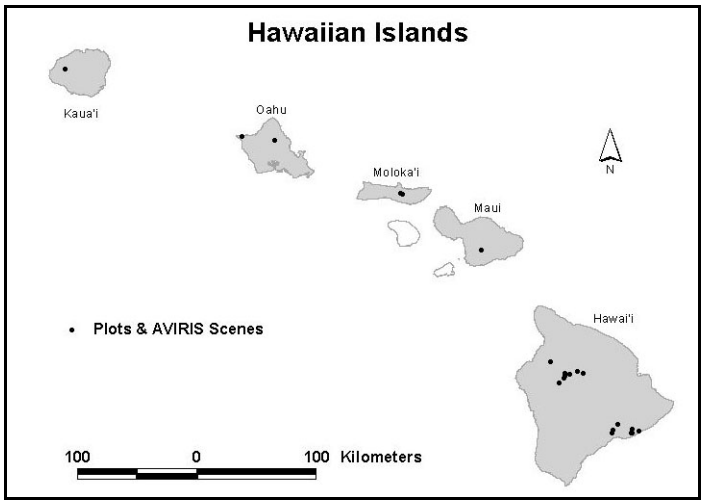

Figure 1. Study islands (shaded) and associated, co-located plot and AVIRIS scene locations.

[1] Department of Geography, University of California, Santa Barbara, California

[2] Forest Fire Laboratory, Pacific Southwest Research Station, USDA Forest Service, Riverside, California

These size classes correspond to 1-hr, 10-hr, 100-hr and 1000-hr fuel moisture time-lag classes, respectively, which are commonly used in fire models (Anderson, 1982). Other dead materials included litter and duff. Live-material biomass included herbaceous components (i.e., forbs, ferns and graminoids) and woody shrubs. Canopy cover had tree, shrub and herbaceous components and is important because it is used in fuel moisture and wind reduction calculations in fire modeling (Albini and Baughman, 1979; Rothermel et al., 1986).

High-altitude AVIRIS data were collected in April, 2000 with a 20-m Ground Instantaneous Field of View (GFOV). Runs were processed to apparent surface reflectance with the MODTRAN radiative transfer model (Green et al., 1993). Reflectance from several field calibration spectra (beaches) were used to remove artifacts in modeled reflectance spectra (Dennison et al., 2001). Calibrated AVIRIS scenes had to be georegistered so that field plots could be located for the sampling of image pixels. Georegistered base information included vector road layers (State of Hawaii, Office of Planning, 1998) and Landsat ETM+ imagery registered to the road vector layer. We georegistered a total of 13 AVIRIS scenes to the UTM projection (Zone 4, Datum WGS 84) with first-order polynomial transformations and nearest-neighbor, 20-m resampling. Transformation equations were built by visually matching points within the AVIRIS imagery to registered points in the Landsat images or the road layer. Root-mean-square error ranged from 0.5 to 1.8 m, using between 5 to 14 points.

Field plots were located in georegistered AVIRIS scenes based on plot-center GPS coordinates. Due to georegistration errors, plot-center location errors, and cloud coverage, the image sampling locations of 10 plots were shifted between 30 to 500 m to locate more appropriate sampling locations. Care was taken to locate the adjusted plot centers in the same vegetation patch.

3. Hyperspectral features analyzed

Spectral mixture analysis (SMA) of AVIRIS data was performed using a 4-endmember (EM) model consisting of green vegetation (GV), non-photosynthetic vegetation (NPV), soil and photogrammetric shade reference EMs. Following techniques outlined by Roberts et al., (1998a), reference EMs were selected from an AVIRIS-convolved library of field spectra (Dennison et al., 2001) according to the criteria that they produced low root-mean-square error (RMSE) and physically-reasonable fractions.

Several vegetation liquid water indices were calculated from AVIRIS reflectance spectra. Equivalent Water Thickness (EWT; Roberts et al., 1998b) was calculated using the water absorption feature between 865 and 1065 nm. The Water Band Index (WI; Peñuelas et al., 1993; Sims and Gamon, 2003) was calculated as R_{900} / R_{970} (the ratio of reflectance (R) at 900 and 970 nm, respectively). The Normalized Difference Water Index (NDWI; Gao, 1996) was calculated as $(R_{860} - R_{1240}) / (R_{860} + R_{1240})$.

Narrowband vegetation indices included the Vegetation Index ($VI = R_{800} / R_{680}$; Sims and Gamon, 2003), Normalized Difference Vegetation Index ($NDVI = [R_{800} - R_{680}] / [R_{800} + R_{680}]$; Sims and Gamon, 2003), Soil-Adjusted Vegetation Index ($SAVI = 1.5 * [R_{800} - R_{680}] / [R_{800} + R_{680} + 0.5]$; Huete, 1988), and the Photochemical Reflectance Index ($PRI = [R_{531} - R_{570}] / [R_{531} + R_{570}]$; Gamon et al., 1997). Landsat ETM+ broadband imagery was simulated using AVIRIS reflectance spectra and the ETM+ spectral response functions for the 6 optical bands. Broadband vegetation indices were then calculated from simulated ETM+ data. These indices included ETM_VI (R_{830} / R_{660}), ETM_NDVI [$(R_{830} - R_{660}) / (R_{830} + R_{660})$], and ETM_SAVI [$1.5 * (R_{830} - R_{660}) / (R_{830} + R_{660} + 0.5)$]. ETM+ indices had the 20-m spatial resolution of the AVIRIS reflectance data.

4. Statistical Analyses

Mean and standard deviation values for reflectance spectra, indices, and SMA output (fractions and RMSE) were calculated from a 3x3-pixel kernel (60 x 60-m = 3600 m^2) centered on each plot. Single- and multiple-regression analyses were used to assess the relationship between field-measured fuel parameters (e.g., 1-hr fuels) and hyperspectral features (e.g., EWT, GV fraction). Analyses included the square-root (SQRT) transformation of the dependent variables (i.e., fuel parameters). SQRT was included as the final model if the adjusted-r^2 value was higher than that without the transformation. For

multiple-regression, the S-Plus 2000 LEAPS step-wise procedure (Mathsoft Engineering & Education, Inc., Cambridge, MA) was used with a minimum Mallow's-C_p criteria to select the best model using all independent variable (i.e., hyperspectral features) combinations. Regression models from LEAPS with fewer variables than the minimum-C_P model were also considered. A lower-variable model was selected if 1) it was significant according to the F statistic (α= 0.05) and 2) a comparison against a higher-variable model was not significant (F-statistic, α= 0.05).

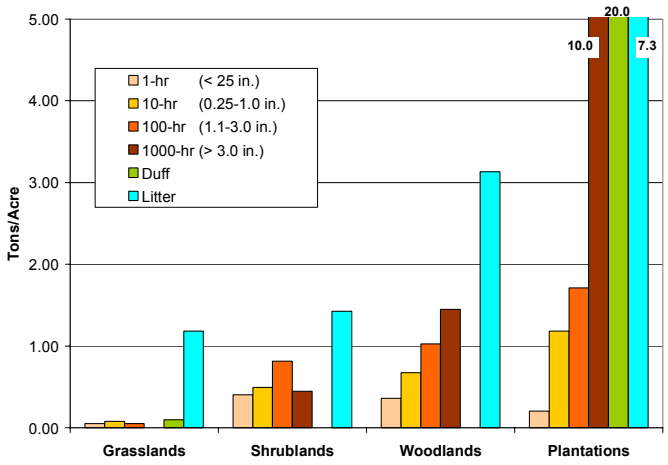

Figure 2. Dead fuels summarized by vegetation type

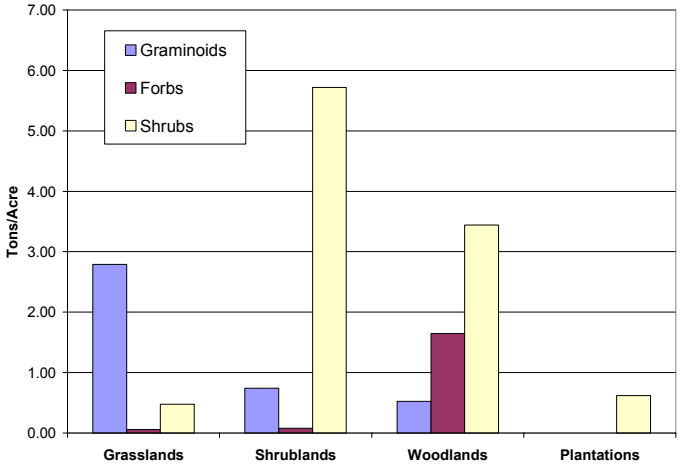

Figure 3. Dead fuels summarized by vegetation type.

5. Results and Discussion

There were significant differences in fuel parameters among the four vegetation types—grasslands, shrublands, woodlands and plantations—for all fuels except for live forb biomass and percent cover of forbs and ferns (Kruskal-Wallis tests; α= 0.05). As is expected, there was a consistent increase in 10-hr, 100-hr, 1000-hr fuels and litter biomass in a gradient of increasing woody vegetation in the grasslands-shrublands-woodlands-plantation sequence (Fig. 2). As would be expected, live-fuel biomass in grasslands was dominated by grasses and dominated by shrubs in shrublands (Fig. 3). Live fuels in woodlands were a mixture of fuel types, and plantations had little live fuels below the tree canopy (Fig. 3).

The G-01 grassland plot was a 1972 pahoehoe lava flow and had trace amounts of vegetation and so its albedo was very low (<10% reflectance; Fig. 4a, G-01). As percent-cover of grass increased, grasslands plot spectra incorporated more grass signal and less soil/lava signal (Fig. 4a). Because grasses were mostly senesced due to an extended El-Niño drought during the April AVIRIS campaign, there was only slight expression of near-infrared (NIR, 700-1300 nm) water absorption features and there was little chlorophyll absorption at 680 nm (Fig. 4a). Shrubs were also strongly affected by the drought during the AVIRIS campaign. Spectra from shrublands plots were dominated by NPV, from exposed branches and twigs, and soil (weathered lava) which was 12-25% exposed (Fig. 4b). There was no evidence of liquid water absorption in the NIR to shortwave infrared (SWIR, 1500-2508 nm) regions, and slight lingo-cellulose absorption was expressed in SWIR (Fig. 4b). Woodlands were a mix of grasses, shrubs and trees. For some plots the dominant spectral signal was from senesced shrubs and grasses (Fig. 4c, W-02, W-04, W-05), similar to shrublands plots. One plot (Fig. 4c, W-06) was located on the wetter southeast side of Hawai'i island and its spectral signal had a strong chlorophyll absorption in visible (VIS, 374-700 nm) and NIR and SWIR water absorption features from Asian swordfern (*Nephrolepsis multiflora*, 92% cover) leaves with high liquid water content. Tree plantation spectra were dominated by radiance that was multiple-scattered in the leaves (mostly needles) of overstory trees (Fig. 4d). There was strong blue (500 nm) and red (680 nm) absorption by chlorophyll, deep expression of NIR liquid water bands (near

975 and 1200 nm), and broad absorption by liquid water in SWIR (Roberts et al., 2004). For plantations, non-photosynthetic dead fuels on or near the forest floor (Fig. 2) are generally shielded by the optically-thick photosynthetic overstory after crown closure has occurred.

Pearson correlation coefficients were calculated by relating dead-fuel parameters to reflectance on a band-by-band basis. Coefficients closely followed the pattern of a photosynthetic overstory canopy (Fig. 5a). For example, red absorption (i.e., lower 680 nm reflectance) associated with chlorophyll tended to be negatively correlated with dead fuels. As mentioned, dead fuels generally increased along the grassland-shrubland-woodland-plantation sequence (Fig. 2), especially for litter, duff and the size-class fuels ≥ 0.65 cm (i.e., ≥ 10 hr). Coincident in this sequence was an increase in overstory volume of photosynthetic material exposed to the sensor. Thus, as overstory cholorphyll increased, so did dead fuel biomass; and subsequently, red reflectance decreased, thereby creating a negative relationship between reflectance and dead fuels. Also, volumetric scattering will increase from grasslands to plantations due to more structure and photosynthetic foliage (e.g., higher leaf area index, LAI) in the plantation overstory. This gradient in scattering will result in increasing NIR reflectance from grasslands to plantations, thereby creating a positive relationship between dead fuel biomass and NIR bands. Because very fine dead materials (< 0.64 cm 1-hr fuels) did not show a strong increase in the grassland-plantation sequence (Fig. 2), these fuels had the weakest correlations across the spectrum (Fig. 5a). There were weaker correlations when considering live fuels (Fig. 5b). Graminoid (i.e., grasses) biomass was strongly positively correlated (r > +0.6) in SWIR bands (1500-2350 nm). There was a negative relationship between tree percent cover and graminoid percent cover, and more tree canopy tended to reduce SWIR reflectance due to water absorption

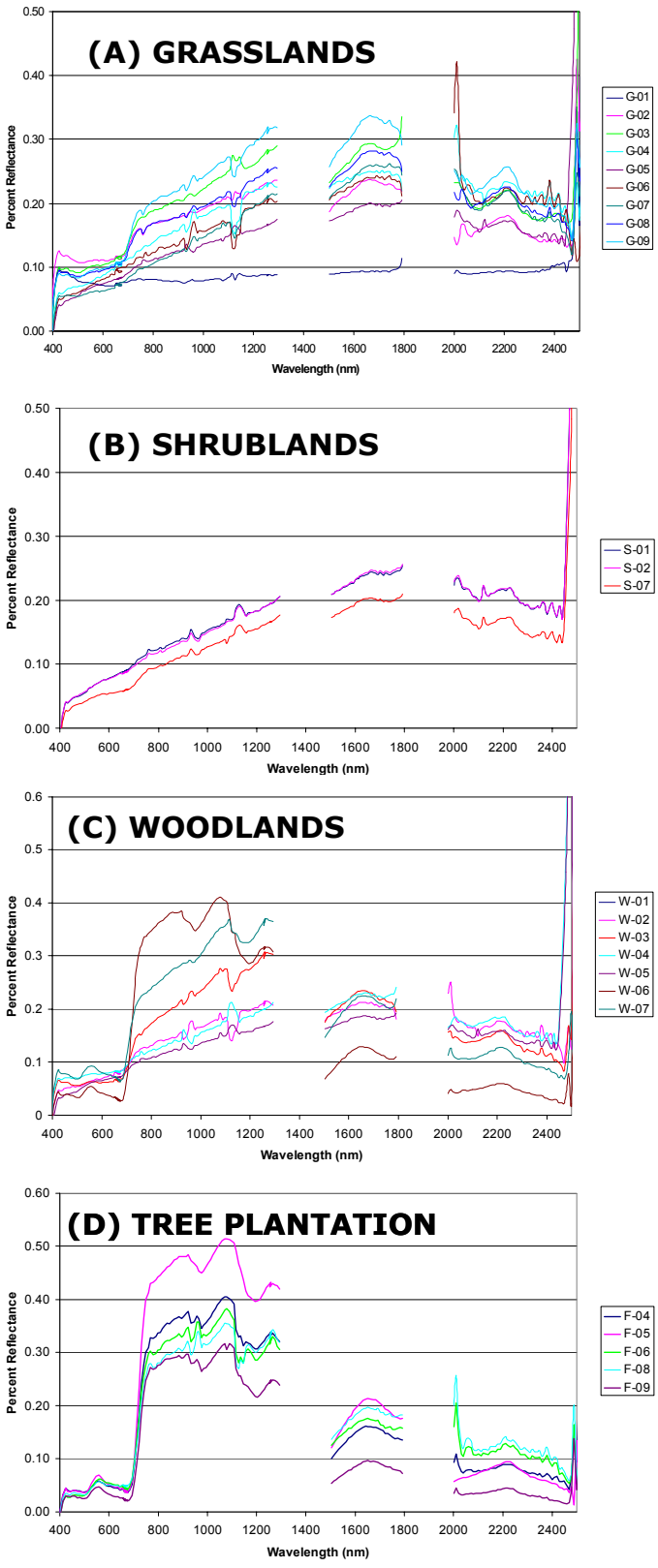

Figure 4. AVIRIS reflectance spectra from plots (average of 9 pixels in 3x3 kernel) for a) grasslands, b) shrublands, c) woodlands, and d) tree plantations.

(Fig. 4d). There is thus a positive relationship between graminoid biomass and SWIR reflectance—with less tree cover, there is more grass cover and more SWIR reflectance.

Relating single AVIRIS-derived variables to fuel parameters, r^2 values ranged from 0.17 to 0.65 (Table 1). The best correlation was +0.80, between litter and NDVI (Fig 6a). This was stronger than the best single-wavelength correlation for litter (r = +0.73, 760 nm, Fig. 5a). NDVI takes advantage of strong spectral contrast seen between 680 and 800 nm wavelengths (Fig. 5a). In ecological terms, higher NDVI may be associated with high LAI (Gong et al., 1995) and more ground litter; and thus, an indirect and positive correlation exists between NDVI and litter biomass. Similar indirect relationships exist for 10-hr and 100-hr fuels, where higher NDVI values are positively correlated with increased structural branches that support plantation overstory leaves (Table 1). These branches are inputs to the layer of dead fuels ≥ 0.65 cm on the surface, thereby creating a positive, indirect relationship between large dead fuels and NDVI (Fig. 6b). A similar argument can be made for the correlation between 1000-hr fuels and PRI, however PRI is expected to be more negative with increasing photosynthetic overstory (Gamon et al., 1997), thus explaining the negative relationship between the variables (Table 1). Duff was associated with plantations (Fig. 2a) and negatively related to NPV (Table 1), indicating that plots with higher percent tree cover shielded more NPV from the sensor.

There was a significant -0.70 correlation between live grass fuels and NDWI (Table 1). If the AVIRIS imagery had been acquired in the wet season, NIR liquid water absorption would be expected to be deeper (higher NDWI) in plantations relative to grasslands due to the multiple-scattering environment of tree canopies, which tend to amplify water absorption features (Roberts et al., 2004). Grass biomass, which decreased from grasslands to plantations (Fig. 2b) would thus be negatively related to NDWI. This relationship may be even stronger in this drought imagery because grass was senesced and so had very low NIR liquid water absorption (Fig. 4a). A similar argument is

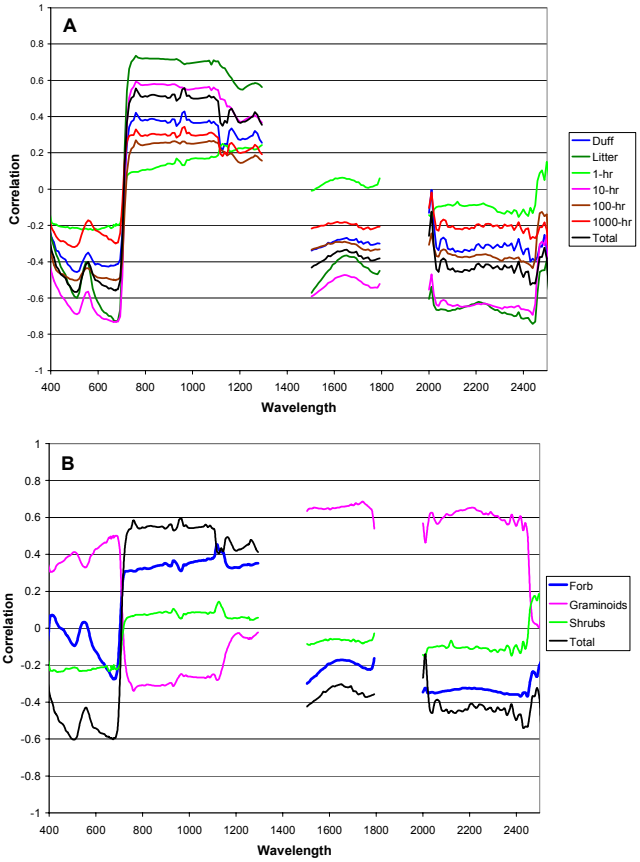

Figure 5. AVIRIS reflectance Pearson's correlation with a) dead fuels and b) aboveground biomass (n=24 plots).

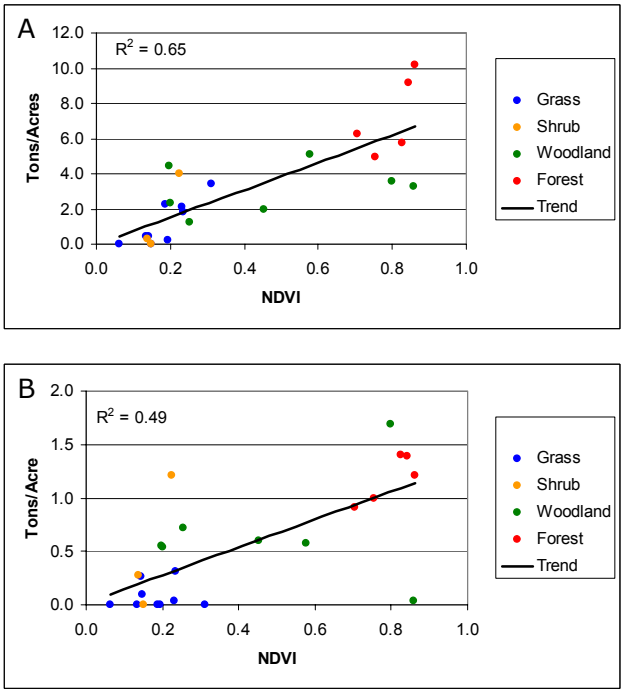

Figure 6. Relationship of narrowband NDVI to a) litter aboveground biomass, b) dead fuels 0.25 to 1 in. biomass.

valid for the strong negative correlation between graminoid percent cover and NDWI (Table 1). As expected, percent tree cover was positively correlated (r = +0.80) to NDVI—with more tree canopy, NDVI increased because there were more photosynthetically-active leaves.

Table 1. Single-variable regression of fuel parameters and AVRIS spectral features.

Dependent	Transform	Independent	R	r^2	Sig
DEAD BIOMASS					
1-hr	None	SOIL	-0.50	0.25	*
10-hr	None	NDVI	0.70	0.49	***
100-hr	Sqrt	NDVI	0.44	0.20	*
1000-hr	Sqrt	PRI	-0.56	0.32	**
Duff	Sqrt	NPV	-0.67	0.44	***
Litter	None	NDVI	0.80	0.65	****
Total	Sqrt	NDVI	0.72	0.52	****
LIVE BIOMASS					
Shrub	Sqrt	SOIL	-0.49	0.24	*
Forb	None	GV	0.52	0.27	**
Graminoid	Sqrt	NDWI	-0.70	0.49	***
Total	Sqrt	SOIL	-0.51	0.26	*
PERCENT COVER					
Tree	Sqrt	NDVI	0.80	0.63	****
Shrub	Sqrt	SOIL	-0.59	0.35	**
Forb & Fern	None	GV	0.41	0.17	*
Graminoid	Sqrt	NDWI	-0.77	0.59	****

Significance levels: * $p \leq 0.05$, ** $p \leq 0.01$, *** $p \leq 0.001$, **** $p \leq 0.0001$, ns= not significant

There were 225 single-variable regression analyses performed (15 dependent vs. 15 independent variables). In terms of the number and significance of correlations against the fuel parameters, NDVI, NPV and PRI were the most useful AVIRIS-derived features (Table 3). NDWI outperformed the WI and EWT liquid water indices and NPV was the best SMA endmember. The Landsat ETM+ (broadband) versions of NDVI (ETM_NDVI) had similar performance as to narrowband NDVI, and ETM_SAVI outperformed narrowband SAVI in terms of the number and significance level of correlations (Tables 2 and 3). There may be other wavelengths to calculate NDVI that could better isolate the red absorption and NIR plateau and outperform the broadband NDVI, however such a sensitivity analysis was beyond the scope of this research. Contrary to expectations, SAVI was not as useful as NDVI for single-variable predictions. It may be that the SAVI soil-baseline parameters need to be better calibrated for the relatively dark lava-derived soil found in our study areas.

The square root transformation of the dependent (fuel) variable improved most multiple-regression equations. Adjusted-R^2 values ranged from 0.22 to 0.83 (Table 4). Equations contained one to four variables and the most common spectral variables used were NDVI, SOIL, RMSE, PRI and SOIL. RMSE was a minor component to the models, but its presence suggests that there is an unmodeled spectral component that is related to the dependent variables. For 1-hr and 10-hr fuels, there was a negative relationship with VI yet a positive relationship with NDVI. It was expected that these variables would provide equivalent information, and it is not clear why they are contradictory. The percent tree cover relationship is the most instructive model. The relationship is associated with negative PRI, positive EWT and negative NPV. As tree cover increases, photosynthetic leaves increase and there is thus less exposed NPV, less PRI, and more water absorption (high EWT).

Table 2. Single-variable regression of fuel parameters and simulated ETM+ vegetation indices.

Dependent	Transform	Independent	R	r^2	Sig
DEAD BIOMASS					
1-hr	None	ETM_NDVI	0.17	0.03	ns
10-hr	None	ETM_NDVI	0.72	0.52	****
100-hr	Sqrt	ETM_NDVI	0.47	0.22	*
1000-hr	Sqrt	ETM_NDVI	0.46	0.21	*
Duff	Sqrt	ETM_NDVI	0.61	0.37	**
Litter	None	ETM_NDVI	0.81	0.65	****
Total	Sqrt	ETM_NDVI	0.73	0.54	****
LIVE BIOMASS					
Shrub	None	ETM_VI	0.40	0.16	ns
Forb	Sqrt	ETM_NDVI	-0.60	0.36	**
Graminoid	None	ETM_NDVI	0.17	0.03	ns
Total	None	ETM_NDVI	0.07	0.00	ns
PERCENT COVER					
Tree	Sqrt	ETM_NDVI	0.79	0.63	****
Shrub	None	ETM_NDVI	0.17	0.03	ns
Forb & Fern	None	ETM_VI	0.40	0.16	ns
Graminoid	Sqrt	ETM_VI	-0.66	0.44	***

Significance levels: * $p \leq 0.05$, ** $p \leq 0.01$, *** $p \leq 0.001$, **** $p \leq 0.0001$, ns= not significant

Table 3. Summary of significant independent variables in single-variable regression analyses.

	$p \leq 0.05$	$p \leq 0.01$	$p \leq 0.001$	$p \leq 0.0001$	Total
NARROWBAND VEGETATION INDICES					
NDVI	2	2	2	4	10
VI	1	5	2	1	9
SAVI	1	2	4	2	9
PRI	3	4	2	1	10
LIQUID WATER INDICES					
EWT	1	1			2
NDWI	1	3	3	1	8
WI		2			2
SPECTRAL MIXTURE ANALYSIS FRACTIONS					
GV	7	2			9
NPV	2	4	2	2	10
SOIL	5	3			8
SHADE	1				1
RMSE	4	1			5
BROADBAND VEGETATION INDICES					
ETM_NDVI	2	2	1	5	10
ETM_VI		4	2	2	8
ETM_SAVI	2	2	1	5	10

Table 4. Multiple-regression analyses of hyperspectral features.

Dependent	Independent Variables	Adj-R^2	Sig.
DEAD BIOMASS			
1-hr*	0.320 - 0.107 x VI + 1.930 x NDVI – 0.002 x RMSE	0.53	**
10-hr*	1.645 - 0.112 x VI + 3.837 x NDVI – 0.014 x GV - 0.005 x RMSE	0.68	***
100-hr*	6.393 - 12.793 x NDWI + 2.936 x NDVI - 0.068 x NPV - 0.004 x RMSE	0.53	**
1000-hr*	-0.529 - 23.293 x PRI	0.32	**
Duff*	-7.180 - 31.428 x PRI + 0.054 x SOIL	0.69	****
Litter*	-0.499 - 4.034 x NDWI + 3.882 x NDVI	0.69	****
LIVE BIOMASS			
Shrub*	3.965 - 0.026 x SOIL	0.24	*
Forb	-3.181 + 0.034 x GV	0.27	**
Graminoid*	-5.497 + 0.193 x VI - 2.901 x NDVI + 0.051 x NPV + 0.006 x RMSE	0.79	****
Total Live*	8.625 - 0.072 x SOIL + 0.010 x RMSE	0.43	**
PERCENT COVER			
Tree	92.774 - 489.078 x PRI + 3.290 x EWT - 0.872 x NPV	0.75	****
Shrub*	11.981 - 0.0790 x SOIL	0.35	**
Forb & Fern	-31.160 + 0.344 x GV	0.22	*
Graminoid	-442.127 + 112.268 x SAVI + 434.492 x PRI + 2.847 x NPV + 1.238 x SOIL	0.83	****

6. Conclusion

In this study we sought to find spectral features that may be useful for estimating important fuel properties as potential per-pixel inputs for fire behavior models. The sizes and spatial distribution of dead surface fuels are the most important components to characterize in these models. In the Hawaiian Islands landscapes analyzed in this study, we found that these dead fuels tended to increase in size and quantity along a grasslands-shrublands-woodlands-tree plantation sequence of vegetation types. Because AVIRIS scenes were acquired during a drought, grasses and shrubs were mostly senesced while tree canopies were green, and so photosynthetic materials exposed to the sensor increased in volume and vigor along the same grasslands to plantation sequence. As tree overstory canopy cover increases, the spectral component of dead surface fuels are a smaller component in the radiance signal reaching the sensor. Therefore, most dead fuels are not directly "sensed" by the sensor, and there is an indirect relationship between reflectance properties of overstory photosynthesis and dead fuel biomass. For this reason, we observed that both narrowband and broadband NDVI was positively correlated with increasing dead fuel size and quantity.

Live-fuel biomass and percent cover were not as well predicted as dead-fuel biomass, even with the inclusion of more variables in the regression models. Grass biomass and cover were well predicted using NDWI with regressions that explained 49% and 59% of the variance, respectively. The negative relationship between moisture content and quantity of grasses exists because grasses were senescent and plantations were not. The relationship would likely be less distinct in wet-season AVIRIS scenes because photosynthetically-active grasses would have deeper NIR liquid water absorption features.

For 10-hr and 100-hr dead fuels, duff, litter, and tree cover, narrowband NDVI provided single-variable models that explained 20% to 65% of the variance. Models were equal or slightly better with broadband ETM_NDVI, indicating that a multispectral satellite may provide adequate sensitivity to these fuel parameters. This is important in an operational sense in that ETM+ data over the whole Hawaiian archipelago are much cheaper and easier to process for producing island-wide fuels maps. For other fuel parameters, such as grass cover, 1000-hr fuels, and duff, we found that features based on AVRIS data were important in single-variable regressions. Multiple regression equations, which used AVIRIS-derived variables, appear stronger based on adjusted-R^2 values. Some variables in these equations, such

as PRI, NDWI and EWT can not be calculated from ETM+ data due to the limited band resolution and/or position. Although SMA fractions can be estimated with ETM+, they should be more accurate when estimated from hyperspectral data. At this stage in our research, we found AVIRIS useful for exploring different indices. However, more field data are required to test model estimation error and establish the relative advantage of hyperspectral data for vegetation fuel estimation. Here we estimated individual fuel parameters (e.g., 10-hr dead biomass), whereas current fire behavior models take more generalized fuel models or types as inputs (Riaño et al., 2002). Future research should focus on methods to map fuel types on a per-pixel basis from estimated fuel parameters, possibly with a decision tree classifier.

7. Acknowledgements

Funding for field work and image analysis was supplied through cooperative agreement No. 01-JV-11272166-136 with the U.S.D.A. Forest Service and through the NASA Solid Earth and Natural Hazards program (NAG2-1140). We also wish to acknowledge the Jet Propulsion Laboratory, which acquired the AVIRIS data used in this study, and supplied the ASD full range spectrometer used for collection of field spectra on the Hawaiian Islands.

8. References

Albini, F. A. and Baughman, R. G. (1979). Estimating windspeeds for predicting wildland fire behavior. USDA Forest Service Res. Pap. INT-221.

Anderson, H. E. 1982. Aids to determining fuel models for estimating fire behavior. USDA Forest Service Gen. Tech. Rep. INT-122.

D'Antonio, C. M. and Vitousek, P. M. (1992). Biological Invasions by Exotic Grasses, the Grass Fire Cycle, and Global Change. *Annual Review of Ecology and Systematics*, *23*, 63–87.

Dennison, P. E., Gardner, M. E., Roberts, D. A., and Green, R. O. (2001). Calibration and vegetation field spectra collection for the 2000 AVIRIS Hawaii deployment. *Summaries of the Tenth Annual JPL Airborne Geoscience Workshop*, Pasadena, California: Jet Propulsion Laboratory.

Finney, Mark A. (1998). FARSITE: Fire Area Simulator—Model development and evaluation. USDA Forest Service Res. Pap. RMRS-RP-4.

Gamon, J. A., Serrano, L. and Surfus, J.S. (1997). The photochemical reflectance index: an optical indicator of photosynthetic radiation use efficiency across species, functional types, and nutrient levels. *Oecologia*, *112*(4), 492–501.

Gao, B. C. (1996). NDWI - A normalized difference water index for remote sensing of vegetation liquid water from space. *Remote Sensing of Environment*, 58(3), 257–266.

Gong, P., Pu, R. L., and Miller, J. R. (1995). Coniferous forest Leaf-Area Index estimation along the Oregon Transect using Compact Airborne Spectrographic Imager data. *Photographic Engineering and Remote Sensing*, 61(9), 1107–1117.

Green, R. O., Conel, J. E., and Roberts, D. A. (1993). Estimation of aerosol optical depth and additional atmospheric parameters for the calculation of apparent reflectance from radiance measured by the Airborne Visible/Infrared Imaging Spectrometer. *Summaries of the Fourth Annual JPL Airborne Geoscience Workshop*, Pasadena, California: Jet Propulsion Laboratory.

Huete, A. R. (1988). A Soil-Adjusted Vegetation Index (SAVI). *Remote Sensing of Environment*, 25(3), 295–309.

Mehroff, L. A. (1998). Endangered and threatened species, in Atlas of Hawai'i, 3rd ed., eds. S. P. Juvik and J. O. Juvik,. University of Hawai'i Press, Honolulu, pp. 150–153.

Peñuelas, J., Filella, I., Biel, C., Serrano, L., and Save,R. (1993). The reflectance at the 950–970 nm region as an indicator of plant water status. *International Journal of Remote Sensing*, *14*, 1887–1905.

Riaño, D., Chuvieco, E., Salas, J., Palacios-Orueta, A., and Bastarrika, A. (2002). Generation of fuel type maps from Landsat TM images and ancillary data in Mediterranean ecosystems. *Canadian Journal of Forest Research*, *32*(8), 1301–1315.

Roberts, D. A., Ustin, S. L., Ogunjemiyo, S., Greenberg, J., Dobrowski, S. Z., Chen, J., and Hinckley, T. M. (2004). Spectral and structural measures of Northwest forest vegetation at leaf to landscape scales. *Ecosystems*, *in press*.

Roberts, D. A., Batista, G. Pereira, J., Waller, E, and Nelson, B. (1998a). Change identification using multitemporal spectral mixture analysis: Applications in eastern Amazonia, *in* Remote Sensing Change Detection: Environmental Monitoring Applications and Methods, eds. C. Elvidge and R. Lunetta, pp. 137–161, Ann Arbor Press, Chelsea, Michigan.

Roberts, D. A., Brownz, K., Green, R., Ustin, S., and Hinckley, T. (1998b). Investigating the relationship between liquid water and leaf area in clonal Populus. *Summaries of the Seventh JPL Airborne Earth Science Workshop.* Pasadena, California: Jet Propulsion Laboratory.

Rothermel, R. C, Wilson, R. A.,Morris, G. A. and Sackett, S. S. (1986). Modeling moisture content of fine dead wildland fuels input to the BEHAVE fire prediction system. USDA Forest Service Res. Pap. INT-359.

Sims, D. A. and Gamon, J. A. (2003). Estimation of vegetation water content and photosynthetic tissue area from spectral reflectance: a comparison of indices based on liquid water and chlorophyll absorption features. *Remote Sensing of Environment*, *84*(4), 526–537.

State of Hawaii Office of Planning. (1998). Hawaii Statewide Geographic Information System. http://www.hawaii.gov/dbedt/gis/ (last accessed 11/01/04).

Wright, C. S., Ottmar, R. D., Vihnanek, R. E., and Weise, D. R. (2002). Stereo photo series for quantifying natural fuels: Grassland, shrubland, woodland, and forest types in Hawaii. USDA Forest Service Gen. Tech. Rep. PNW-GTR-545.